Dynamic criticality at the jamming transition

Atsushi Ikeda,[1] Ludovic Berthier,[1] and Giulio Biroli[2]

[1] *Laboratoire Charles Coulomb, UMR 5221, CNRS and Université Montpellier 2, Montpellier, France*
[2] *Institut de Physique Théorique (IPhT), CEA, and CNRS URA 2306, 91191 Gif-sur-Yvette, France*

(Dated: September 14, 2012)

We characterize vibrational motion occurring at low temperatures in dense suspensions of soft repulsive spheres over a broad range of volume fractions encompassing the jamming transition at ($T = 0$, $\varphi = \varphi_J$). We find that characteristic time and length scales of thermal vibrations obey critical scaling in the vicinity of the jamming transition. We show in particular that the amplitude and the time scale of dynamic fluctuations diverge symmetrically on both sides of the transition, and directly reveal a diverging correlation length. The critical region near φ_J is divided in three different regimes separated by a characteristic temperature scale $T^\star(\varphi)$ that vanishes quadratically with the distance to φ_J. While two of them, ($T < T^\star(\varphi)$, $\varphi > \varphi_J$) and ($T < T^\star(\varphi)$, $\varphi < \varphi_J$), are described by harmonic theories developed in the zero temperature limit, the third one for $T > T^\star(\varphi)$ is inherently anharmonic and displays new critical properties. We find that the quadratic scaling of $T^\star(\varphi)$ is due to nonperturbative anharmonic contributions, its amplitude being orders of magnitude smaller than the perturbative prediction based on the expansion to quartic order in the interactions. Our results show that thermal vibrations in colloidal assemblies directly reveal the critical nature of the jamming transition. The critical region, however, is very narrow and has not yet been attained experimentally, even in recent specifically-dedicated experiments.

PACS numbers: 05.10.-a, 05.20.Jj, 64.70.qj

I. INTRODUCTION

Important theoretical efforts have recently been devoted to the study of the jamming transition and the critical properties of the so-called J-point [1]. An important feature of a system approaching the jamming transition is the emergence of a peculiar density of states which differs from the ones of ordinary solid materials. The studies of athermal packings of soft repulsive particles above the jamming transition [2–7], and of hard particles below jamming [8] both unveiled that the density of states acquires an excess of modes at low frequencies, and thus increasingly differs from the usual Debye behavior as jamming is approached. The presence of an excess of harmonic modes which are distinct from usual plane waves has been proposed as an explanation to many unusual low-temperature properties of disordered materials [1].

Motivated by these theoretical results, several recent experiments aimed at measuring the vibrational motion of a variety of dense colloidal assemblies [9–15]. Experimentally, the normal modes are accessed by diagonalizing the displacement correlation matrix to obtain quantitative information about time scales (eigenvalues) and length scales (eigenvectors) of the vibrational motion. These experimental studies were made possible through the development of increasingly accurate tools to record single particle motion in colloidal assemblies. Similar studies for standard molecular glasses are not possible since particle motion cannot be visualized directly in that case, but vibrational motion can also be accessed in systems such as driven granular media, where attempts to characterize modes were recently reported [16].

We wish to characterize the relation, if any, between these two sets of efforts. Are the normal modes determined in experimental work related to the ones studied theoretically and numerically near the jamming transition? What are the necessary conditions to observe experimentally the 'low-frequency' or 'soft' modes discussed theoretically? What are the real space signatures in single particle trajectories of the anomalous density of states that develops near jamming?

More fundamentally, these questions raise the issue of the validity of a harmonic description of the dynamics of amorphous materials at low temperature. Indeed, theoretical studies are performed in the zero-temperature limit where a harmonic description (or an effective one for hard spheres [8]) is justified. On the other hand experiments are inevitably performed at finite temperatures in colloidal systems, or under gentle vibrations for granular materials. Therefore, understanding to what extent finite temperatures affect the theoretical predictions and quantifying the role of anharmonicity are two important problems which are tackled by the present work.

The fact that finite temperature can be an extremely singular perturbation close to jamming can easily be grasped recalling that an excess of low energy modes may lead to large fluctuations which can eventually destabilize the system, as it happens for two-dimensional crystals [17]. For the jamming problem, there exist two possibilities: (1) The harmonic description remains valid at low enough temperature. Then, the flat density of states would imply arbitrarily large fluctuations and would suggest the melting of the disordered solid, which would then invalidate a purely harmonic description. (2) The harmonic description breaks down approaching the jamming transition *at any value of the temperature*. This would allow the existence of a disordered solid but would also imply that anharmonicity is crucial to prevent the solid

from breaking apart. In both cases, the conclusion is that the harmonic description must break down at any finite temperature close enough to φ_J. Because experimental [9, 11, 12, 14, 15] and numerical [18–21] works show that close to jamming a disordered solid is stable, the second possibility is clearly the correct one, and anharmonicity must play an increasing role approaching the jamming transition. This issue was recently discussed in Refs. [5, 22, 23], but our conclusions will differ somewhat from these earlier studies.

In this work we provide a complete description of the role of finite temperatures and anharmonicity on the critical behavior close to the jamming transition and the understanding of the connection, or the lack thereof, between vibrational properties studied in experiments and theory. We explain when it is correct to assume that thermal vibrations and eigenmodes of the dynamical matrix coincide, and the range of parameters where single particle motion becomes dominated by genuine 'soft' or 'low-frequency' modes of the type discussed in the context of the jamming transition. This issue is also important theoretically, as it could help us to understand better the validity of analytical replica calculations where thermal fluctuations are taken into account [24, 25], but vibrational eigenmodes are not directly described.

Finally, because we focus on thermal fluctuations, we cannot, in principle, address the more complicated situation where particle motion does not result from an equilibrium thermal bath, as is the case in granular media [16, 23]. However, the type of 'vibrational heterogeneity' that we reveal through the study of thermal vibrations is strongly reminiscent of the findings reported in two distinct experimental studies of dynamic heterogeneity in driven granular media across the jamming transition [26, 27]. In particular, we obtain at finite temperature a nonmonotonic dependence of both a dynamic susceptibility and a correlation length scale very similar to the experimental findings for dissipative grains. They stem, in our case, from the existence of a correlation length that is divergent when the temperature is strictly zero. Surprisingly, this divergent length scale is physically distinct from the 'isostatic' length scale which is central to the description of the density of states near jamming [2], or the response function of athermal packings [28]. We will connect this last finding with recent investigations of random networks [7].

This paper is organized as follows. In Sec. II we describe our numerical model and methods. In Sec. III, we present numerical results for the dynamic behavior of low-temperature packings of soft repulsive spheres across the jamming density. In Sec. IV, we analyze more precisely the scaling behavior of these dynamic quantities, and the emergence of diverging time scales and length scales near jamming. In Sec. V, we show that these divergences result from the existence of diverging dynamic fluctuations and of a diverging correlation length scale. The finite temperature critical behavior is analyzed in Sec. VI. In Sec. VII we numerically determine the temperature scale for the emergence of anharmonicity, and provide a theoretical analysis of its physical content. Finally, we use our findings to discuss experimental results in Sec. VIII.

II. MODEL AND NUMERICAL METHODS

We use molecular dynamics simulations to study the thermal vibrations of sphere packings near the jamming transition. We focus on monodisperse harmonic spheres [29], interacting through a pairwise potential,

$$v(r_{ij}) = \frac{\epsilon}{2}(1 - r_{ij}/\sigma)^2\Theta(\sigma - r_{ij}), \qquad (1)$$

where $\Theta(x)$ is the Heaviside function and σ is the particle diameter. We use system sizes between $N = 120$ and $N = 64000$ particles imposing periodic boundary conditions, changing the volume V to adjust the packing fraction $\varphi = \pi\sigma^3 N/(6V)$. The main results are reported for $N = 8000$, while we use larger and smaller systems for specific purposes to be specified below. We use Newtonian dynamics, and integrate Newton's equation of motion in the microcanonical ensemble after proper thermalization of the system at the desired temperature. The results are reported in units of $\sqrt{m\sigma^2/\epsilon}$ for time scales, of σ for length scales, and of ϵ/k_B for temperatures, where k_B is the Boltzmann constant.

To produce a low temperature amorphous packing of harmonic spheres in three dimensions at volume fraction φ, we first perform an instantaneous quench from $T = \infty$ to $T = 10^{-5}$ (well below the glass temperature [18]) at a large volume fraction, $\varphi = 0.70$. We then let the system relax and rapidly settle in a metastable state. At these very low temperatures (compared to the glass temperature) aging effects rapidly become negligible and the system simply performs vibrations near a well-defined energy minimum.

We then explore the (φ, T) phase diagram of these packings by decreasing T and φ to the desired values. Using this method we can follow *the same jammed configuration* with different particle overlap or gap when changing temperature or density. For each independent quench, the jamming density φ_J is therefore well-defined and can be measured very accurately [30, 31], for instance by decompressing the packing at $T = 0$ towards φ_J and measuring the volume fraction where the pressure vanishes. Following previous work [20], we mainly discuss the vibrational behavior of a single, large packing with $N = 8000$ and for which $\varphi_J \simeq 0.6466$. We provide additional data for different packings where necessary. We checked that the results reported in this work do not depend on the specific choice of a packing.

Note that all dynamic observables discussed in this paper are measured after aging effects have terminated, and are thus stationary or independent of the waiting time, even though the dynamics is not ergodic. We

merely explore the statistical properties of a representative metastable state. Thus, our studies are qualitatively distinct from the non-stationary aging dynamics studied in Ref. [8], and from the athermal studies of Refs. [32–34] where an externally imposed shear flow affects the structure and dynamics of the packings.

III. DYNAMICAL BEHAVIOR AT FINITE TEMPERATURES NEAR JAMMING

A. Mean-squared displacement

In order to characterize vibrational motion, we focus on single particle dynamics. The most basic correlation function is the mean-squared displacement (MSD), which is easily measured experimentally in colloidal systems,

$$\Delta_0^2(t) = \frac{1}{N}\sum_{i=1}^{N}\langle|\Delta\mathbf{r}_i(t)|^2\rangle, \qquad (2)$$

where $\Delta\mathbf{r}_i(t) = \mathbf{r}_i(t) - \mathbf{r}_i(0)$, and $\mathbf{r}_i(t)$ represents the position of particle i at time t. The brackets in Eq. (2) represent an average over long trajectories performed at a given T and φ (but nevertheless restricted to a single metastable state). We will be particularly interested in the long-time limit of the MSD, which we call the Debye-Waller (DW) factor.

Near the jamming transition, there is a slight technical problem arising in these measurements because the packings produced numerically contain a small fraction of 'rattlers', that have peculiar dynamic properties since they are less connected than most particles and therefore have distinct dynamical properties. An annoying feature is that rattlers move much more than the other particles, and so they might completely dominate the sum in Eq. (2), thus yielding results which do not reflect the representative behavior of the system.

We used two distinct methods to prevent rattlers from spoiling the measurements. A first, simple method consists in computing a modified version of the MSD,

$$\Delta_{\rm mod}^2(t) = \frac{1}{N}\sum_{i=1}^{N}\frac{3}{\langle|\Delta\mathbf{r}_i(t)|^{-2}\rangle}, \qquad (3)$$

which gives nearly no statistical weight to the particles that move much further than the average. The prefactor 3 in the definition (3) is such that $\Delta_{\rm mod}^2(t) = \Delta_0^2(t)$ when the distribution of single particle displacement is Gaussian. In a second method, we directly remove the rattlers and measure

$$\Delta^2(t) = \frac{1}{N'}\sum_{i=1}^{N'}\langle|\Delta\mathbf{r}_i(t)|^2\rangle, \qquad (4)$$

where N' is the total particle number which are not rattlers. Although rattlers can be defined unambiguously in the jammed regime, $\varphi > \varphi_J$, by measuring contact numbers in the ground state at $T = 0$, we cannot apply this method to the unjammed regime, $\varphi < \varphi_J$. We have applied the following procedure which can be used in both regimes. We first measure the DW factor of each particle. We then calculate the median value, which is less affected by rattlers than the averaged value. Then we regard the particles whose DW factor is 5 times larger than the intermediate value as rattlers. We have confirmed that this procedure and the analysis at the ground state give the same result in the jammed regime. We have also confirmed that the definitions Eqs. (3) and (4) yield similar results at all densities and temperatures. We note that definition (3) is conceptually extremely simple and does not require any empirical criterion to identify rattlers, and could therefore be very useful for the analysis of experimental data. In the following, we present the data obtained from the definition (4).

In Fig. 1, we present typical results for the behavior of the MSD obtained at constant temperature, $T = 10^{-8}$, and a range of volume fraction encompassing the jamming density φ_J. The time dependence of the MSD is typically characterized by two distinct time scales. At very short times, the MSD is purely ballistic and follows $\Delta^2(t) = Tt^2$, which simply results from the short-time integration of Newton's equation of motion for particles thermalized at temperature T. Deviations from this trivial behavior occur after a microscopic time scale, τ_0, which corresponds to the time where particles start to feel the influence of their neighbors. This is indicated by the open squares in Fig. 1. We shall characterize τ_0 more accurately in Sec. IV A below, but the data in Fig. 1 indicate that τ_0 decreases with φ.

For times $t > \tau_0$, the time evolution of the MSD crosses over to an intermediate time regime where it obeys diffusive behavior, before saturating at long times to a plateau, the DW factor $\Delta^2(\infty)$, which decreases rapidly upon compression. The approach to the plateau value occurs after a typical time scale, $t^\star$, marked by the filled squares in Fig. 1. The precise definition of $t^\star$ is also discussed below. The data indicate again that $t^\star$ decreases strongly when the system is compressed. The fact that the DW factors remain finite in the long-time limit shows that our systems are genuine amorphous solids [35], and that they do not melt despite having a flat density of states at $T = 0$ and $\varphi = \varphi_J$.

We now extract the Debye-Waller factor from the long-time limit of the mean-squared displacements. We gather our results for a broad range of densities and temperatures in Fig. 1. We find that the DW factor decreases upon compression at fixed temperature, mirroring the behavior of both time scales τ_0 and $t^\star$. When the system gets denser, the particles have less space to move, their vibrations are more constrained, and so the typical amplitude of the vibrations and the related time scales become smaller. Therefore, a smooth evolution of dynamic quantities with density can be anticipated from trivial reasons, unrelated to the specific physics of the

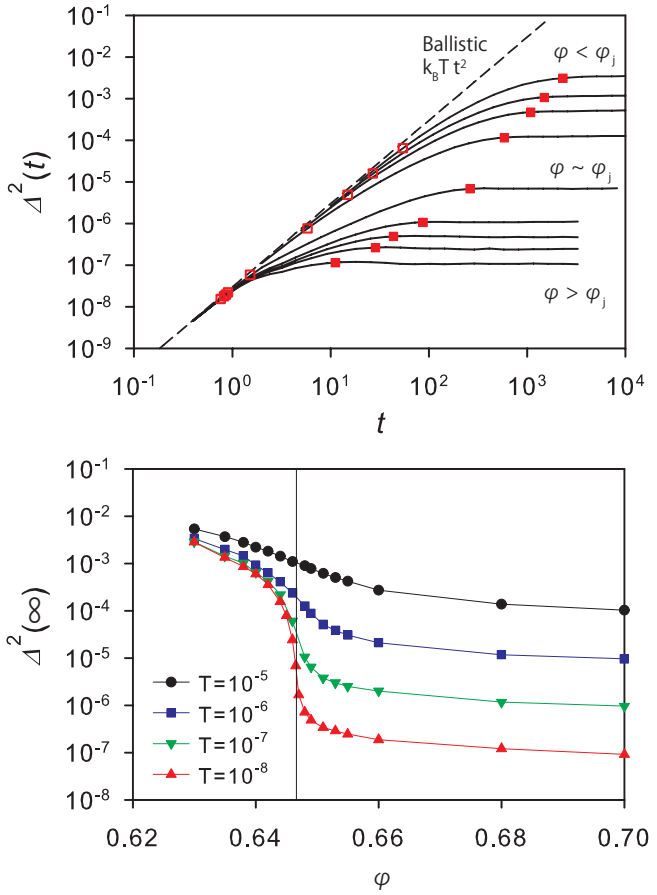

FIG. 1: Top: Time dependence of the mean-squared displacements (MSD) at constant temperature, $T = 10^{-8}$, and various volume fractions increasing from top to bottom across the jamming transition. Open squares indicate the microscopic time scale τ_0, filled squares indicate the long timescale $t^\star$, which marks roughly the convergence of the MSD to its long-time limit. Both time scales decrease with φ, but their ratio is maximum near φ_J. Bottom: Volume fraction dependence of the Debye-Waller (DW) factor (long-time limit of the MSD) for different temperatures. The $T = 0$ jamming singularity at $\varphi_J \approx 0.6466$ (vertical line) strongly influences the DW factor when T becomes very small, $T < 10^{-7}$, and φ is very close to the critical density, $0.64 < \varphi_J < 0.655$.

jamming transition.

Two interesting features emerge from the DW data in Fig. 1. Firstly, the scaling with temperature is different on both sides of the jamming transition. This is not surprising, as many other observables have a similar dual behavior [25], which corresponds to the two different situations obtained when $T \to 0$. While the system corresponds to a hard sphere assembly when $\varphi < \varphi_J$, it is instead a jammed soft solid for $\varphi > \varphi_J$. Accordingly, the DW factor converges to its hard sphere value below jamming and remains finite as $T \to 0$, while it vanishes linearly with T above jamming, as in ordinary solids [17].

Secondly, we also note that as T becomes smaller, the volume fraction dependence of the DW factor becomes more and more singular in the vicinity of φ_J, which suggests that some singularity will emerge in the $T \to 0$ limit, to be discussed below. Here, we simply emphasize that for the harmonic sphere system, temperature must be at least lower than $T = 10^{-7}$ (in units of the spring constant ϵ) to notice the emergence of a singular volume fraction dependence of the DW factors near the jamming transition. For larger temperatures, the DW factor smoothly depends on T and φ as a result of the compression but the jamming singularity does not manifest itself. Anticipating the discussion of experimental work to come in Sec. VIII, we also remark that a singular behavior can be seen in the data when the DW factors take extremely small values, typically $\Delta^2(\infty) < 10^{-4}$ (in units of the particle size), which corresponds to resolving distances with a precision greater than $\sigma/100$, which can be technically quite challenging since it corresponds to about 10nm for colloids with $\sigma = 1\mu$m.

B. Velocity autocorrelation and density of states

Another way of looking at single particle motion is to record the velocity autocorrelation function defined by

$$d(t) = \frac{1}{3N'T} \sum_{i=1}^{N'} \langle \mathbf{v}_i(t) \cdot \mathbf{v}_i(0) \rangle, \tag{5}$$

where $\mathbf{v}_i(t)$ denotes the velocity of particle i at time t. Note that we again remove rattlers from the definition in Eq. (5). When Fourier transformed, this becomes what we (abusively) call the 'density of states' (DOS) [36]:

$$d(\omega) = \int_0^\infty dt \cos(\omega t) d(t). \tag{6}$$

Note that $d(\omega)$ can be measured arbitrarily far from the harmonic limit and so it does not represent a genuine density of states, but it does reduce to the true DOS (as measured by diagonalizing the dynamical matrix) when the harmonic approximation holds [23]. Below, we will carefully determine when this assumption is correct. Note also that by definition one has

$$d(t) = \frac{1}{2} \frac{\partial^2 \Delta^2(t)}{\partial t^2}, \tag{7}$$

which shows that both types of measurements (density of states and mean-squared displacements) are directly related and, in fact, contain nearly equivalent information. This remark suggests that, when carefully analyzed, the MSD themselves should directly reveal the anomalous features of the DOS, as we shall demonstrate.

In Fig. 2, we present the frequency dependence of $d(\omega)$ at the same set of temperatures and densities as in Fig. 1. At low frequency, one gets the expected Debye behavior, $d(\omega) \sim \omega^2$ for our three-dimensional systems. Moving to larger frequencies, we see that the DOS exhibits a single peak below jamming, $\varphi < \varphi_J$, and this peak broadens

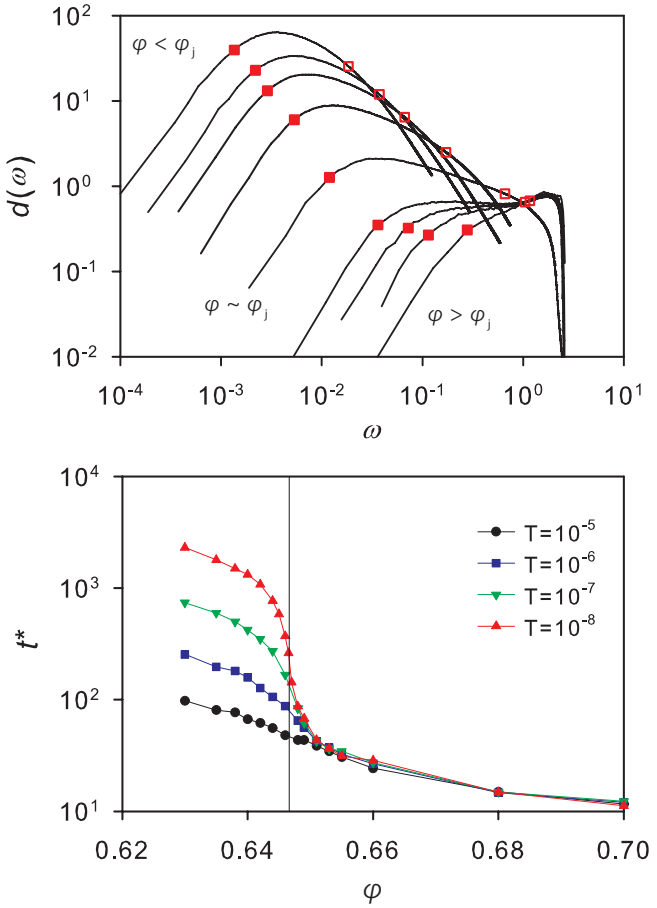

FIG. 2: Top: Frequency dependence of the density of states at constant temperature, $T = 10^{-8}$, and densities increasing from top to bottom. Parameters are as in Fig. 1. Open squares indicate the microscopic frequency $\omega_0 = \pi/\tau_0$, while filled squares indicate the low-frequency crossover $\omega^\star = \pi/t^\star$. Bottom: Volume fraction dependence of $t^\star = \pi/\omega^\star$ for different temperatures. The vertical line indicates φ_J.

with increasing density and transforms into a plateau in the jammed regime, $\varphi > \varphi_J$. To determine the position of this low-frequency characteristic behavior over the entire density range, we define the crossover frequency $\omega^\star$ as the peak position of the quantity $d(\omega)/\omega$. In Fig. 2 we indicate the frequency $\omega^\star$ with filled squares, which appear as good indicators of the low-frequency crossover towards the Debye power law. Clearly, $\omega^\star$ shifts to larger frequency when φ increases.

At large frequency, $d(\omega)$ undergoes a second crossover towards either an algebraic $d(\omega) \sim \omega^{-2}$ behavior below jamming, or towards an even steeper decay above jamming. This behavior simply mirrors a qualitative change in the short-time behavior of the velocity autocorrelation function from exponential to Gaussian over the same density range [37]. We report the microscopic frequency $\omega_0 = \pi/\tau_0$ as open squares in Fig. 2, which confirms that τ_0 governs the high-frequency crossover in the DOS.

The comparison between the MSD and DOS in Figs. 1 and 2 confirms that both quantities contain equivalent information in the sense that they both reveal that vibrational dynamics is controlled by two distinct time scales, $\tau_0 = \pi/\omega_0$ and $t^\star = \pi/\omega^\star$. The former indicates when particles start to feel their neighbors and deviations from ballistic motion appear. The latter corresponds to the convergence of the MSD to its long-time limit, and also to a crossover to a Debye behavior in the DOS, meaning that interesting dynamics arises in the range $\tau_0 \ll t \ll t^\star$, or $\omega^\star \ll \omega \ll \omega_0$ in the frequency domain.

Note also that the DOS reported in Fig. 2 are fully consistent with previous determination in both jammed [3] and unjammed regimes [8]. The main feature noticed in previous work in these DOS data is the emergence of the low-frequency crossover $\omega^\star$, which we can alternatively interpret, in the time domain, as the time it takes for the MSD to reach its plateau value, see Fig. 1.

We extract $t^\star = \pi/\omega^\star$ for a broad range of volume fractions and temperatures, see Fig. 2. As in the case of the DW factor, $t^\star$ shows very different temperature dependence in jammed and unjammed regimes. It is nearly independent of temperature in the jammed regime but scales as $t^\star \sim \sqrt{T}$, reflecting the fact that temperature trivially renormalizes the unit time scale in hard sphere systems. As temperature gets lower, we observe that $t^\star$ acquires a strong density dependence very close to φ_J, changing by several orders of magnitude over a narrow density range. By contrast, $t^\star$ changes smoothly when T is not low enough, as a consequence of the compression.

IV. CRITICAL BEHAVIOR

In the previous section, we discussed the qualitative behavior of various time scales characterizing the vibrational motion of dense packings of harmonic spheres. In particular, we noticed that singular density dependences seem to emerge when temperature decreases. In this section, we focus on these low-temperature singularities and show that they correspond to zero-temperature algebraic divergences rounded by finite temperature effects, and therefore to an underlying critical dynamics.

A. Elementary time scales and length scales

From the data reported in Figs. 1 and 2, one finds that the dynamics shows an abrupt crossover at low temperature when φ_J is crossed. Without further analysis, it is however not obvious to decide when a nontrivial critical behavior becomes manifest, as compression itself influences the dynamics. This suggests that one should first renormalize time scales and length scales in terms of the microscopic ones. In the case of the jamming transition, compared to usual critical phenomena, this is particularly important since the dynamics below and above jamming are very different: dynamical behaviors are trivial for $\varphi \ll \varphi_J$ and $\varphi \gg \varphi_J$ but in a quite distinct way.

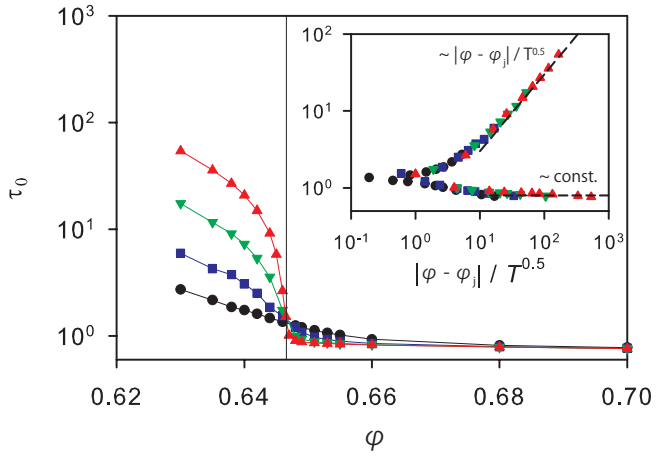

FIG. 3: Volume fraction dependence of the microscopic time scale τ_0, Eq. (8), at various temperatures decreasing from bottom to top. The vertical line indicates φ_J. These data were used to draw the open squares in Figs. 1 and 2. Inset: τ_0 is replotted as a function of the scaling variable $|\varphi - \varphi_J|/\sqrt{T}$. Upper and lower dashed lines correspond to $T \to 0$ limits for hard and soft spheres, respectively, Eqs. (9, 10).

Our first step is to analyze the short-time dynamics in order to understand the behavior of the microscopic time scale τ_0 discussed above, which also sets the high-frequency cutoff in the DOS $d(\omega)$. In practice, we measure τ_0 by analyzing the short-time decay of the velocity autocorrelation function $d(t)$ in Eq. (5), and quantitatively determine τ_0 from the definition

$$d(t = \tau_0) = 1/e. \tag{8}$$

The data for τ_0 are shown in Fig. 3. These data were also used to determine the position of the open squares in the MSD data of Fig. 1, and in the DOS data of Fig. 2.

The short-time behavior of the velocity autocorrelation function $d(t)$ is very different in jammed and unjammed regimes at low temperature. In the zero-temperature limit, $d(t)$ display an exponential decay when $\varphi < \varphi_J$ due to two-body collisions in the hard sphere limit, whose characteristic time scale can be deduced from Enskog theory (roughly the time it takes to a particle to collide ballistically with a neighbor) [37],

$$\frac{1}{\tau_0} \simeq \frac{8\rho g(\sigma^+)}{3}\sqrt{\frac{\pi T}{m}} \sim \frac{\sqrt{T}}{|\varphi - \varphi_J|}, \tag{9}$$

where the final approximation only holds very close to jamming. We stress that this two-body collision time scale decreases very rapidly as φ_J is approached from below because the typical gap between neighboring particles also vanishes rapidly, scaling as $(\varphi - \varphi_J)$. This is quantitatively taken into account in Eq. (9) through the contact value of the pair correlation function, $g(\sigma^+)$.

In the low temperature limit above jamming, $\varphi > \varphi_j$, $d(t)$ shows instead a Gaussian decay, whose characteristic timescale can now be estimated as the inverse of the Einstein frequency [17],

$$\frac{1}{\tau_0} \simeq \sqrt{\frac{\rho}{3m}\int d\mathbf{r} g(r)\nabla^2 v(r)} \sim \text{const}, \tag{10}$$

where $g(r)$ is the pair correlation function, and the final approximation means that τ_0 has no singular dependence upon either T or φ near jamming.

The data in Fig. 3 indicate that τ_0 interpolates smoothly between the two limits discussed above on both sides of the transition at finite temperatures. The main panel confirms that it is proportional to $\sqrt{T}$ below jamming, and becomes independent of temperature in the jammed regime. As in the case of $t^\star$, it is only in the very low temperature limit that a singular density dependence emerges. In the inset of Fig. 3, τ_0 is replotted as a function of the rescaled variable $x = |\varphi - \varphi_J|/\sqrt{T}$, in order to reconcile the behavior on both sides, as is the case for most observables near jamming [18, 25, 32]. Indeed we get a very good collapse of all the data along two distinct branches, confirming the simple dependences discussed above. We emphasize that even though τ_0 is controlled by relatively simple physics and it simply sets the microscopic time scale for the dynamics, it changes rather dramatically near jamming at low temperatures.

Having identified the elementary time scale τ_0 on both sides of the jamming transition, we shall now focus on the elementary length scale. Below jamming, as discussed above, particles move ballistically over the typical interparticle distance in a time τ_0. Thus, the elementary length scale obtained by ballistic motion reads:

$$\ell_0 = \sqrt{T}\tau_0. \tag{11}$$

The same relation holds on the other side of the jamming transition. In that case the elementary length scale is given by the typical displacement due to a harmonic mode with Einstein frequency (10), leading again to Eq. (11). In both cases, ℓ_0 represents the distance travelled ballistically over the microscopic time scale τ_0.

In conclusion, in this section we have identified the elementary length scales and time scales, Eqs. (9, 10, 11), which characterize noncollective dynamics. In the next section we shall show that approaching the jamming transition, there emerge time scales and length scales which actually become much larger than τ_0 and ℓ_0, thus signalling the existence of *bona fide* collective dynamics.

B. Critical behavior of adimensional data

We now reconsider the dynamical behavior studied in Sec. III and analyze the data obtained by renormalizing all observables in terms of the elementary time scales and length scales.

We define a rescaled Debye-Waller factor as

$$\Delta_\infty(\varphi, T) \equiv \frac{\Delta^2(\infty)}{\ell_0^2} = \frac{\Delta^2(\infty)}{T\tau_0^2}. \tag{12}$$

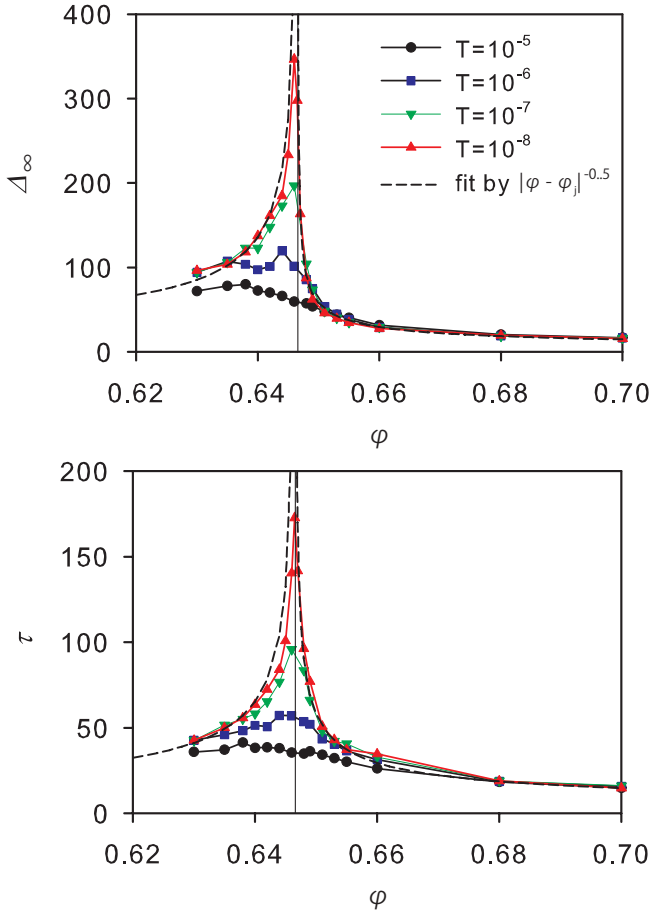

FIG. 4: Critical behavior for rescaled dynamic observables. Top: Rescaled Debye-Waller factor, Eq. (12). Bottom: Rescaled time scale for vibrational motion, Eq. (13). In both panels, dashed lines represent the critical divergence $\sim |\varphi - \varphi_J|^{-1/2}$, Eq. (18), and the vertical line indicates φ_J.

and we similarly renormalize the long time scale $t^\star$ in terms of τ_0:

$$\tau(\varphi, T) \equiv \frac{t^\star}{\tau_0}. \tag{13}$$

A visual interpretation of these adimensional quantities can be given from the symbols in Fig. 1, since Δ_∞ and τ respectively quantify the vertical and horizontal distances between the filled and open squares, i.e. between the short-time and long-time dynamics.

The numerical data for these two quantities are reported in Fig. 4. Clearly, they both are smooth functions of the density when temperature is not very low (but still much smaller than the glass temperature), e.g. $T = 10^{-5}$, and $T = 10^{-6}$, and they also are smooth functions of the temperature when φ is not in the immediate vicinity of φ_J. This implies that in this regime, the 'low-frequency' crossover $\omega^\star$ is not very 'low', i.e. not strongly decoupled from the natural microscopic time scale τ_0. In the similar vein, in the non-critical regime the DW factor is not very much larger than its natural scale, and thus thermal vibrations are neither 'anomalous' nor characterized by 'soft' modes which would reflect an underlying nontrivial or collective dynamics.

The situation becomes more interesting at very low temperature, $T \leq 10^{-7}$ and for densities near jamming, $0.64 \leq \varphi \leq 0.655$, because adimensional quantities may become very large, and additionally they acquire a nonmonotonic density dependence across φ_J, strongly suggesting the existence of divergences as $T \to 0$ on both sides of the transition. Thus, we conclude that the anomalous 'low-frequency' behavior of the DOS approaching jamming corresponds to the appearance of an adimensional timescale τ that becomes large, $\tau \gg 1$, and an 'anomalously' large adimensional amplitude of the vibrational motions, $\Delta_\infty \gg 1$. Thus, when analyzed from the viewpoint of thermal vibrations, the jamming transition is *accompanied by a critical slowing* down which we now confirm through a scaling analysis. In Sec. V, we will show that this slowing down is also accompanied by a diverging correlation length.

C. Critical behavior and scaling in the $T \to 0$ limit

We now connect the two critical behaviors found above and estimate the corresponding $T \to 0$ divergences using a scaling analysis. This analysis amounts to assuming that slow vibrational motion is controlled by a single dominant timescale, t^*, *i.e.* that the DOS at low frequency has a non-trivial scaling behavior of the form

$$d(\omega) = \tau_0 f_\pm\left(\frac{\omega}{\omega^\star}\right), \qquad \omega \ll 1/\tau_0, \tag{14}$$

where $f_\pm(x)$ corresponds to the universal behavior of the density of state below $(-)$ and above $(+)$ jamming, respectively. We checked that numerical data are consistent with this scaling assumption. Both functions $f_\pm(x)$ are proportional to x^2 for $x \to 0$ in order to recover the usual Debye law. For $x \to \infty$, $f_+(x)$ tends to a constant to recover the flat part of the density of states, while $f_-(x)$ decreases to reproduce the hard sphere behavior [50].

By definition of the MSD and of the DOS we get

$$\Delta^2(t) = 6T \int_0^\infty d\omega \frac{d(\omega)}{\omega^2}[1 - \cos(\omega t)]. \tag{15}$$

In the long-time limit, the scaling behavior in Eq. (14) yields

$$\Delta^2(\infty) \approx \frac{T\tau_0}{\omega^\star} \int_0^\infty dx \frac{f_\pm(x)}{x^2}, \tag{16}$$

which simply implies that

$$\Delta_\infty \sim \tau. \tag{17}$$

This result unveils that, to leading order, the data in both panels of Fig. 4 are in fact equivalent, up to a numerical prefactor stemming from the difference in the scaling

functions $f_{\pm}(x)$ expressed by Eq. (16). The result in Eq. (17) has a simple physical interpretation, because it says that a large amplitude for vibrational motions develops near jamming, and that the time it takes for particles to fully explore these vibrational degrees of freedom also becomes larger, the scaling between (adimensional) times and lengths obeying a simple diffusive scaling.

Finally, by using literature results concerning the scaling of $\omega^\star$ approaching the jamming transition at $T = 0$ [2, 8], we find that τ diverges symmetrically on both sides of φ_J as $|\varphi - \varphi_J|^{-1/2}$. For our rescaled variables, this implies that when $T \to 0$

$$\Delta_\infty \sim \tau \sim |\varphi - \varphi_J|^{-1/2}, \tag{18}$$

on both sides of the jamming transition. These scaling laws are in good agreement with our data, as shown with dashed lines in Fig. 4. We have not tried to measure the exponent in Eq. (18) directly to detect a possible deviation from the value $-\frac{1}{2}$, but our numerical results suggest that this correction, if it exists, is quite small, in agreement with recent numerical work [8, 21].

As is clear Fig. 4, the divergence is cut off by using a finite temperature. As we shall discuss later, this is due to the appearance of anharmonicity at finite temperatures.

V. DIVERGING CORRELATION LENGTH

In the previous section, we found that the amplitude of the vibrational motion, and the associated time scale, may become nontrivial, i.e. much larger than the expected elementary values corresponding to non-collective dynamics. It is therefore natural to expect some kind of diverging correlation length scale. It is the purpose of this section to unveil and study this correlation length.

A. Four-point correlation function

Since we identified the mean-squared displacement as the quantity of interest to pinpoint the existence of the transition, we now seek spatial correlations between the particle displacements during the vibrational motion. This amounts to measuring the extent of spatial correlations in the dynamics of glassy states. We can therefore use the machinery developed to study dynamic heterogeneity in glassy materials [38]. First, we measure the following four-point susceptibility

$$\chi_4(t) = N\left[\langle \mu(t)^2\rangle - \langle \mu(t)\rangle^2\right], \tag{19}$$

defined as the variance of the spontaneous fluctuations of the instantaneous value of the volume-averaged mobility $\mu(t)$, defined as

$$\mu(t) = \frac{1}{N}\sum_{i=1}^{N} \frac{|\Delta \mathbf{r}_i(t)|^2}{\langle |\Delta \mathbf{r}_i(t)|^2\rangle} - 1. \tag{20}$$

Note that the thermal average in the denominator of Eq. (20) does not include an average over particles, and thus particles with larger displacements do not dominate the sum in the definition of $\mu(t)$. This implies in particular that rattlers are not dramatically affecting the numerical measurements of $\chi_4(t)$.

While $\chi_4(t)$ measures the total amplitude of spatial correlations, direct access to a correlation length scale is provided by the spatially resolved correlator, which we study in the Fourier space:

$$S_4(q,t) = \frac{1}{N}\sum_{j,k=1}^{N} \langle \left|\mu_j(t)\mu_k(t)e^{i\mathbf{q}\cdot\mathbf{r}_{jk}}\right|\rangle, \tag{21}$$

where $\mathbf{r}_{jk} = \mathbf{r}_j(0) - \mathbf{r}_k(0)$ is the separation between particles j and k at $t = 0$ and $\mu_j(t)$ is the contribution of particle j to the mobility, $\mu_j(t) = |\Delta \mathbf{r}_j(t)|^2/\langle |\Delta \mathbf{r}_j t)|^2\rangle - 1$.

Two remarks before showing our results. First, we have included all particles in the analysis of the dynamic heterogeneity, because the rattlers do not dominate the sum in Eqs. (19, 21), contrary to the MSD. We have numerically checked that our results in this section are identical if we remove the rattlers. Second, our definition of $\chi_4(t)$ does not explicitly involve a 'probing' length scale as in other works [26, 38]. In fact, using the mobility defined in Eq. (20) is equivalent to selecting automatically the appropriate probing length at each time [26].

We find that $\chi_4(t)$ increases with t at short times, but it does not display a clear maximum at intermediate times as is usually found in systems near a glass transition [39], but saturates to a long-time limit discussed below. Here we wish to characterize the spatially heterogeneous dynamics relevant for Δ_∞ and τ. We therefore concentrate on time scales of the order of $t^\star$ discussed above, and we measure

$$\chi_4(\varphi, T) \equiv \chi_4(t = t^\star), \tag{22}$$

and the corresponding structure factor:

$$S_4(q; \varphi, T) \equiv S_4(q, t = t^\star). \tag{23}$$

Representative numerical results are shown in Fig. 5. As for the adimensional quantities Δ_∞ and τ in Fig. 4, χ_4 also shows a striking nonmonotonic density dependence across φ_J, which becomes more pronounced as T decreases, and would seem to diverge on both sides of the jamming transition as $T \to 0$. These results strongly suggest that the slowing down and excess amplitude of thermal vibrations are the result of collective, spatially correlated dynamics. Remark again that χ_4 acquires a strong nonmonotonic density dependence in the close vicinity of φ_J, but only for temperatures which are at least below $T \approx 10^{-7}$, while it remains nearly constant and rather insensitive to the underlying jamming transition everywhere else. Finally, remark that the critical behaviour of χ_4 emerges in Fig. 5 without further analysis or normalization by an elementary 'correlation unit' [51]. This

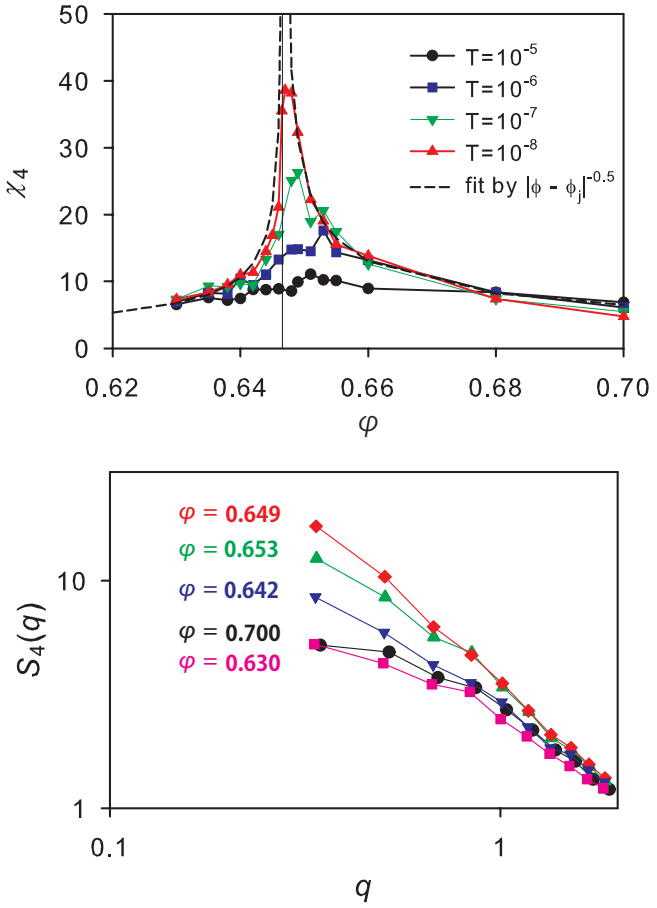

FIG. 5: Top: Volume fraction dependence of the dynamic susceptibility $\chi_4(t = t^\star)$, Eq. (22), for various temperatures showing the emergence of 'vibrational heterogeneity' at low enough T close to φ_J (shown with the vertical line). Bottom: Four-point correlator $S_4(q, t = t^\star)$ at $T = 10^{-8}$ and various volume fractions exhibits a nonmonotonic density dependence (note the nonmonotonic evolution of the φ labels).

makes it a very relevant quantity to be measured experimentally, as it directly reveals the dynamic criticality associated to the jamming transition.

We now focus on spatial correlations to extract the corresponding correlation lengh scale over which thermal vibrations occurring over a time scale $t^\star$ are correlated. In Fig. 5, we present the evolution of $S_4(q)$ for $T = 10^{-8}$ across the jamming density. As suggested by the behavior of χ_4, we find that $S_4(q)$ is also characterized by a nonmonotonic behavior with φ, spatial correlations being modest at both low and large φ, and being maximum near φ_J. Note that $S_4(q \to 0)$ represents the volume integral of the spatial correlation between particle displacement, and it is thus natural that the low-wavevector limit of $S_4(q)$ follows the same trend as χ_4 [40]. However, the spatially resolved correlator allows us to directly extract a correlation length through the q dependence of $S_4(q)$. Clearly, the approach to the low-q plateau occurs for lower q when $\varphi \approx \varphi_J$, which indicates that the corresponding correlation length is also maximum there at finite T, and would diverge at φ_J in the $T \to 0$ limit.

Before discussing the divergence at $T = 0$ in more detail, we wish to emphasize the striking similarity between the numerical results displayed in Fig. 5 quantifying the the 'vibrational heterogeneity' of our thermally excited packings of soft particles, and a similar nonmonotonic dynamic heterogeneity reported for gently vibrated grains in Refs. [26, 27]. Although the excitation mechanisms and the physical systems are quite distinct, it is very tempting to suggest that both sets of measurements are actually probing the same underlying dynamic criticality associated to the jamming transition.

B. Critical behavior and scaling in the zero temperature limit

We now connect these observations of spatially heterogeneous vibrational dynamics with the critical behavior of τ and Δ_∞, extending the previous scaling analysis. Our starting point to evaluate χ_4 is to assume that fluctuations are Gaussian and, hence, four-point correlation functions can be written as products of two-point functions. This is correct within the harmonic approximation, which is valid in the zero-temperature limit we are considering for this analysis. With this assumption, we can obtain an analytical expression of the long-time limit, $t \to \infty$, of the four-point susceptibility as

$$\chi_4(t \to \infty) \approx \left(\frac{T}{\Delta^2(\infty)}\right)^2 \int_{\omega_{\min}} d\omega \frac{d(\omega)}{\omega^4}. \qquad (24)$$

Here $\omega_{\min}$ is the lowest frequency of the density of state for a given system. When the system size becomes large, $\omega_{\min} \sim L^{-1} \to 0$ and $d(\omega) \propto \omega^2$ for small ω, and then, the integral displays an infrared divergence which is cut-off at a system size dependent value, as we have numerically confirmed. This is because the lowest frequency mode is a plane wave for which the motion of all the particles in the system are fully correlated [39].

We focus instead on finite times, $\chi_4 = \chi_4(t = t^*)$:

$$\chi_4(t^*) \approx \left(\frac{T}{\Delta^2(t^*)}\right)^2 \int_{\omega^\star} d\omega \frac{d(\omega)}{\omega^4}, \qquad (25)$$

from which we deduce

$$\chi_4 \sim \frac{1}{d(\omega^\star)\omega^\star} \sim \tau. \qquad (26)$$

Finally, if we assume (to be confirmed in a short while) an Ornstein-Zernike form for the correlation length we also obtain the relation between susceptibility and length scale, $\xi_4 \sim \sqrt{\chi_4}$.

To summarize our scaling analysis, we have shown that the following quantities are all connected in a simple way at the level of their scaling behaviors, and we obtained the following critical scalings:

$$\Delta_\infty \sim \tau \sim \chi_4 \sim \xi_4^2. \qquad (27)$$

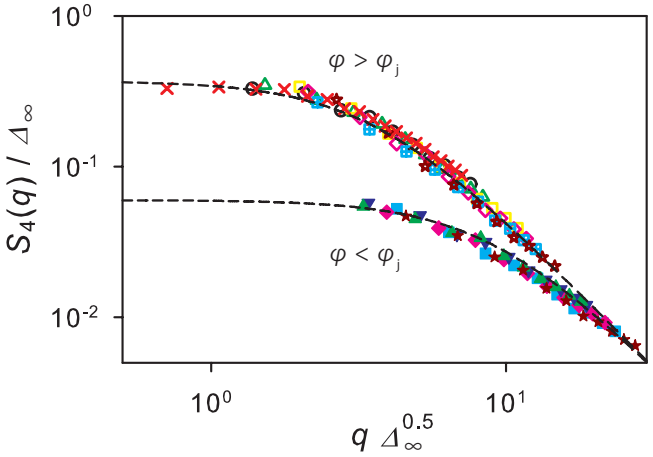

FIG. 6: Test of the scaling behavior of $S_4(q)$ using the assumption that $\xi_4 \sim \sqrt{\Delta_\infty}$. Note that this data collapse involves no free parameter since S_4 and Δ_∞ result from indepent measurements. Dashed lines are fits to the Ornstein-Zernike functional form, Eq. (28).

Note that in order to derive these results we only used the harmonic approximation (valid when $T \to 0$) and the scaling assumption (14). If we add the information, obtained numerically in Refs. [2, 8], that τ diverges as $|\varphi - \varphi_J|^{-1/2}$ then we also get the zero temperature divergence of $\Delta_\infty \propto |\varphi - \varphi_J|^{-1/2}$ and of $\xi_4 \propto |\varphi - \varphi_J|^{-1/4}$ approaching the jamming transition. As discussed before and is clear from our data, any finite temperature cuts off these divergences.

According to our analysis, the diverging correlation length is proportional to the square root of the diverging excess amplitude of the thermal vibrations, $\xi_4 \sim \sqrt{\Delta_\infty}$. We directly test this hypothesis in Fig. 6 where we present $S_4(q)/\Delta_\infty$ as a function of $q\sqrt{\Delta_\infty}$. Clearly, all the data are collapsed very well along two branches corresponding to both sides of the jamming transition. We emphasize that this data collapse involves no adjustable parameter, but makes use of two independent sets of measurements. Additionally, we show that both branches are correctly described by an Ornstein-Zernike wavevector dependence, namely

$$S_4(q) \approx \frac{c_\pm \Delta_\infty}{1 + c_\pm q^2 \Delta_\infty}, \tag{28}$$

with $c_\pm$ a numerical prefactor which is distinct for the two branches. These data directly confirm the validity of the analysis in Eq. (27).

We conclude that the appearance of 'anomalously' slow and large vibration motion is also associated with spatially heterogeneous dynamics, which is a form of *dynamic criticality* [41]. These observations indicate that the jamming transition appears as a genuine critical transition with both a critical slowing down and a diverging length scale. Since the slowing down occurs for thermal vibrations, this suggests that a convenient order parameter to describe the transition is the vibrational motion within cages deep into the glassy phase. It is intriguing that all the critical exponents describing time scales, amplitude of vibration, and dynamic heterogeneity are related in a trivial manner, Eq. (27). Interestingly these divergences are symmetric and hold quantitatively for both hard and soft spheres, provided adimensional quantities are considered.

We note that the length scale quantifying the spatial correlations in the excess amplitude of the vibrations diverges, for the harmonic potential used in this study, as

$$\xi_4 \sim |\varphi - \varphi_J|^{-1/4}. \tag{29}$$

A length scale diverging with the same exponent was already discussed in different contexts. In Ref. [3], a diverging length is identified from the transverse structure factor of the normal modes obtained for soft spheres above jamming. This length scale also appears in the analysis of Ref. [6] of the heat transport in jammed solids. Finally, the same length scale also shows up in a mean-field treatment of the localization length of the elastic response of model networks [7]. To our knowledge, for hard spheres, this length scale was not discussed before. Surprisingly, in both soft and hard cases, the isostatic length scale introduced in Ref. [2] does not directly appear in any of the physical quantities we discuss in this work. Finally, ξ_4 in Eq. (29) seems to differ also from the correlation lengths measured in Refs. [32, 42, 43].

Remark that in our scaling analysis, arguments involving the average contact number are not directly employed. It is only to obtain the divergences of τ, Δ_∞, and ξ_4 with $|\varphi - \varphi_J|$ that we made use of the scaling of $\omega^\star$ with $|\varphi - \varphi_J|$ which was related to the distance to isostaticity [2]. We stress that none of those divergences is fully understood theoretically from a microscopic viewpoint. In fact, isostatic arguments [2] trace back the behavior of ω^* with $|\varphi - \varphi_J|$ to the one of the contact number, which is not directly derived, but measured from numerical simulations. An alternative theoretical approach, which is fully microscopic, uses statistical mechanics and replica calculations to study the jamming transition [24]. When applied to harmonic spheres [20, 25], it correctly predicts that the jamming transition is characterized by a diverging amplitude of thermal vibrations: $\Delta_\infty \sim |\varphi - \varphi_J|^{-1}$. However, this predicted divergence is only qualitatively correct, and the predicted critical exponent is wrong, see Eq. (27). It would be interesting to understand better the source of this discrepancy from the replica viewpoint [44]. Our results also suggest that the theory should be reconsidered in order to make precise predictions for a diverging correlation length and dynamic susceptibility associated to the jamming transition.

VI. FINITE TEMPERATURE CRITICAL BEHAVIOR

In the following we will fully describe the critical behavior in the (φ, T) phase diagram at the jamming transi-

tion. We will first analyze the low-T harmonic regimes in both jammed and unjammed phases. We shall show that their domain of validity is restricted to a temperature regime that shrinks approaching φ_J. This corresponds to an emergent temperature scale, $T^\star(\varphi)$, that vanishes quadratically with $|\varphi - \varphi_J|$. Finally, we shall focus on the finite temperature critical regime, corresponding to $T^\star \ll T \ll 1$, that is related to the critical divergences when $T \to 0$ for $\varphi = \varphi_J$.

A. Regime I: Harmonic description above jamming and its domain of validity

In the following we shall establish that approaching the jamming transition from the jammed phase, the harmonic description used in the previous section is valid and allows one to explain the behavior of physical observables related to vibrational motions if temperature is low enough. Moreover, we shall find the temperature scale, $T^\star(\varphi)$, above which the harmonic description breaks down and the low temperature physical behavior changes.

To this end, we first focus on the temperature dependence of the DOS measured via Eq. (5) for $\varphi > \varphi_J$. Typical data are shown in Fig. 7 together with $T = 0$ result obtained from the diagonalization of dynamical matrix in the ground state at $T = 0$. We observe that by increasing the temperature, deviations from the $T = 0$ result emerge and become more pronounced. Notice, in particular, that it is near the high-frequency cutoff that deviations appear first when T increases. By normalization, the low-frequency part of the DOS is then also affected. Qualitatively similar results were shown in Ref. [4].

For the particular density shown in Fig. 7, we observe that the DOS converges to its $T \to 0$ limit when $T < T^\star \approx 10^{-7}$. Thus, by contrast to the results of Ref. [22] we conclude that *a finite temperature region exists* where the harmonic approximation holds.

To quantify the size of this harmonic regime, we measure the changes in $d(\omega)$ through its first moment:

$$\omega_1(\varphi, T) = \int_0^\infty d\omega \, d(\omega)\omega. \tag{30}$$

The observed change in $d(\omega)$ suggest that ω_1 should decrease with increasing T, because the DOS gives less weight to large frequencies when T increases.

Our numerical analysis fully confirms this expectation, see Fig. 7. We find that, for any given density $\varphi > \varphi_J$, the first moment ω_1 decreases above some crossover temperature $T^\star$, which depends strongly on the volume fraction. To see this, we rescale in the lower panel of Fig. 7 the first moment ω_1 by its value at $T = 0$, and present its evolution as a function of the rescaled temperature $T/T^\star$. Our numerical results are consistent with a simple behavior

$$\frac{\omega_1(\varphi, T)}{\omega_1(\varphi, T = 0)} \approx \mathcal{W}\left(\frac{T}{T^\star}\right), \tag{31}$$

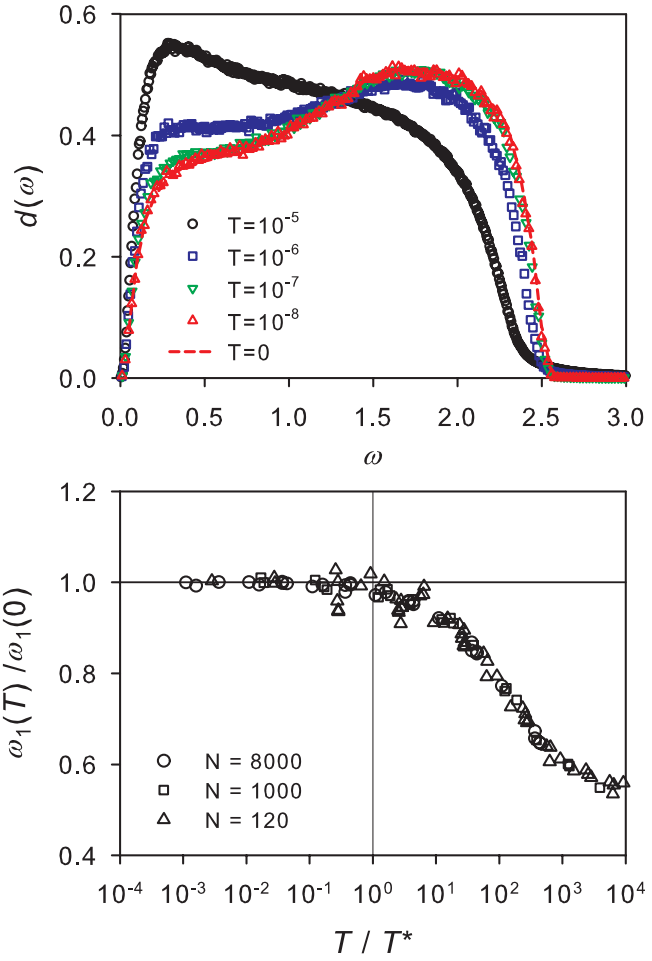

FIG. 7: Limit of validity of harmonic approximation above jamming. Top: The density of state $d(\omega)$ at $\varphi = 0.655$ ($\varphi - \varphi_J \approx 0.0084$) measured for various temperatures through Eq. (5). The $T = 0$ DOS is obtained from diagonalization of the dynamical matrix. Bottom: Convergence of the first moment of the density of state to its $T = 0$ limit below a crossover temperature scale $T^\star = 10^{-3}(\varphi - \varphi_J)^2$ which is independent of system size. The vertical line indicates $T/T^\star = 1$.

where $\mathcal{W}(x \to 0) = 1$, with

$$T^\star \approx a(\varphi - \varphi_J)^2, \tag{32}$$

where $a \simeq 10^{-3}$ is a numerical prefactor. There is an ambiguity in the absolute value of the numerical coefficient a, since the scaling collapse in Fig. 7 does not depend on it. We have determined a such that $\mathcal{W}(x)$ starts to show deviations from 1 when $x \approx 1$.

To fully demonstrate that a harmonic regime exists in the thermodynamic limit, we must make sure that $T^\star$ does not decrease to zero as the system size N is increased. Indeed, a strong system size dependence of the onset of anharmonicity was reported in Ref. [22]. To test this idea, we have repeated the above measurements for various system sizes, $N = 120$, 1000, and 8000. As shown in Fig. 7 we find that our results are devoid of any

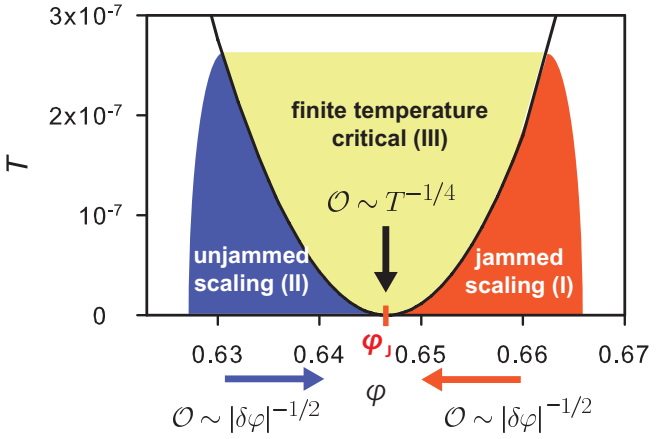

FIG. 8: The structure of the three scaling regimes where power law divergences and 'anomalous' vibrational motion is observed. Regimes I and II are described by $T = 0$ harmonic theories, while dynamics in Regime III is fully anharmonic. These regimes are separated by the crossover temperature $T^\star \sim 10^{-3}(\varphi - \varphi_J)^2$ discussed in Sec. VII. Note the small range of parameters where the effect of the $T = 0$ jamming critical point are felt and Eqs. (34, 37) hold.

system size dependence, although the statistical noise is of course larger for smaller systems.

The fact that $T^\star$ vanishes quadratically with $(\varphi - \varphi_J)$ for all system sizes confirms that materials exactly at φ_J are 'marginally' solid with special properties. In particular, the linear response and harmonic approximation regimes have a vanishing domain of validity [5, 45]. Our results seem consistent with the analysis of low-energy barriers performed numerically in Ref. [5]. In particular, we conclude that the $T = 0$ DOS cannot be used at φ_J to infer properties of the vibrational dynamics at any finite temperature. This resolves the problem raised in the introduction. The material does not 'melt' at jamming when thermal fluctuations are added, because a finite amount of thermal noise pushes the system in a anharmonic regime preventing the system from breaking apart.

In conclusion, we find that for $\varphi > \varphi_J$ and $T < T^\star(\varphi)$ the density of states converges to its zero temperature limit which is correctly described by the harmonic approximation. In this regime the critical behavior is the one discussed previously in the zero temperature limit. We shall call this part of the phase diagram 'Regime I', see Fig 8. Above the temperature scale $T^\star(\varphi)$ the harmonic approximation breaks down and the critical behavior crosses over to Regime III that we discuss later. An explanation for the quadratic scaling of $T^\star(\varphi)$ is presented in Sec. VII.

B. Regime II: Effective harmonic description below jamming and its domain of validity

Below jamming, the $T \to 0$ limit inherently produces a strongly anharmonic system, because it produces hard

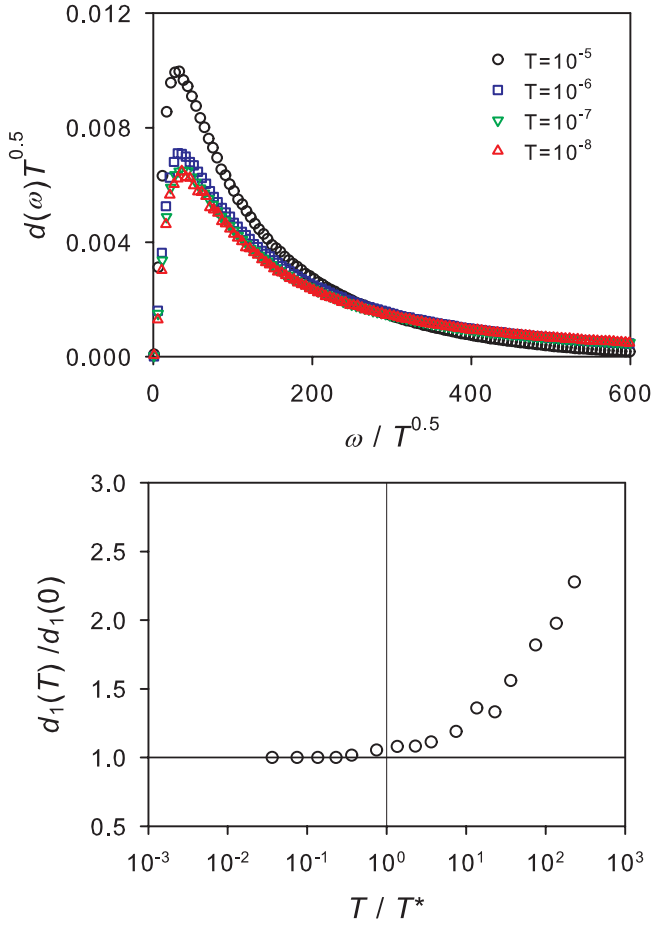

FIG. 9: Limit of validity of (effective) harmonic approximation below jamming. Top: Temperature-scaled density of state $d(\omega)\sqrt{T}$ at $\varphi = 0.630$ and various temperatures converges to $T = 0$ limit below $T^\star \approx 10^{-7}$. Bottom: Convergence of the height of the first peak of the DOS to its $T = 0$ value below the crossover temperature scale $T^\star(\varphi) = 10^{-3}(\varphi_J - \varphi)^2$. The vertical line indicates $T/T^\star = 1$.

sphere packings with zero energy, and the Hessian is not defined. However, an effective harmonic description that describes this behavior for $\varphi < \varphi_J$ can be approximately obtained [8]. In this section we repeat the analysis performed in Regime I to determine the limit of validity of the effective harmonic description below jamming, which defines 'Regime II' in the phase diagram, see Fig. 8.

In Fig. 9, we characterize the temperature evolution of the DOS at fixed volume fraction and decreasing temperature at $\varphi = 0.63 < \varphi_J$. To remove a trivial temperature dependence of the time scale for hard spheres, we plotted $d(\omega)/\sqrt{T}$ versus $\omega\sqrt{T}$, as it is this rescaled DOS which eventually becomes independent of T as $T \to 0$.

Again, we observe that the DOS actually converges to its $T \to 0$ limit for this particular density below $T^\star \approx 10^{-7}$. To quantify the extent of the hard sphere regime, we focus on the height of the first peak of the DOS, $d_1(T)$, which is a very sensitive indicator of the temperature evolution of $d(\omega)$. As in the case of the first

moment above jamming, we follow the convergence $d_1(T)$ to its $T = 0$ value, and determine the crossover temperature $T^\star(\varphi)$ controlling this convergence, see Fig. 9. The numerical results show that there is a again a simple behavior for this quantity,

$$\frac{d_1(\varphi, T)}{d_1(\varphi, T = 0)} \approx \mathcal{D}\left(\frac{T}{T^\star}\right), \tag{33}$$

where $\mathcal{D}(x \to 0) = 1$ with $T^\star$ taken from the previous section. As in the case of jammed phase, there is a slight ambiguity in the actual prefactor of $T^\star$. For the unjammed region, we simply use the a value determined for the jammed region, and find that this works very well.

In conclusion, we find that for $\varphi < \varphi_J$ and $T < T^\star(\varphi)$ the density of states converges to its zero temperature limit which is correctly described by the effective harmonic approximation [8]. In this Regime II, the critical behavior is the one discussed previously in the zero temperature limit, see Fig 12. For $T > T^\star(\varphi)$ the harmonic approximation breaks down and the critical behavior crosses over to Regime III that will be discussed in the following. An explanation for the quadratic scaling of $T^\star(\varphi)$ will be presented in Sec. VII.

C. Regime III: Anharmonic critical regime at finite temperature

We found in previous sections that below the temperature scale $T^\star(\varphi)$, which vanishes quadratically and symmetrically in $|\varphi-\varphi_J|$ approaching the jamming transition from both sides, the critical behavior is well described by the harmonic theory, which leads to symmetric divergences on both sides of φ_J, captured by

$$\Delta_\infty \sim \tau \sim \chi_4 \sim \xi_4^2 \sim |\varphi - \varphi_J|^{-1/2} \tag{34}$$

We also showed that a finite temperature cuts off these divergences. This means that at $\varphi = \varphi_J$ all these observables are finite but diverge as $T \to 0$. This represents a distinct critical regime which cannot be described by the harmonic approximation, and which is therefore controlled by anharmonicity and finite temperatures. We call this 'Regime III', see Fig 8.

In order to obtain scaling laws in this regime, we use scaling arguments and assume that the behavior of the physical observables on both sides of the jamming transition is connected via (observable-dependent) scaling functions [18, 32]:

$$\mathcal{O}(\varphi, T) = \frac{1}{|\varphi - \varphi_J|^{1/2}} \mathcal{H}_\mathcal{O}\left(\frac{\varphi - \varphi_J}{\sqrt{T}}\right), \tag{35}$$

where $\mathcal{O}$ stands for any of the following observables: Δ_∞, τ, χ_4 or ξ_4^2. The three regimes I, II, and III described in the phase diagram in Fig 12 correspond respectively to $x \gg 1$, $x \ll -1$, and $|x| \ll 1$. Therefore, the scaling functions must be such that:

$$\mathcal{H}_\mathcal{O}(x) \to c_\mathcal{O}^\pm, \quad x \to \pm\infty, \tag{36}$$

in order to recover the correct $T = 0$ divergences characteristic of regimes I and II, respectively; $c_\mathcal{O}^\pm$ are observable-dependent numerical constants.

The critical behavior in regime III can then be obtained by requiring that when $\varphi \to \varphi_J$ at small but finite temperature the dependence on $\varphi - \varphi_J$ drops out from Eq. (35). In this way, one finds that at $\varphi = \varphi_J$:

$$\Delta_\infty \sim \tau \sim \chi_4 \sim \xi_4^2 \sim T^{-1/4} \tag{37}$$

The critical behaviors of the three regimes are summarized in Fig. 8. Note that contrary to regimes I and II, physical or microscopic interpretation for the divergences in Eq. (37) are missing. A possible path could be the extension of the effective harmonic description of Ref. [8] to continous potentials, but this is beyond the scope of this work.

VII. ANHARMONICITY AND THE TEMPERATURE SCALE $T^\star$

We have found by numerical simulations that the harmonic description for the jammed and unjammed phase breaks down below a characteristic temperature scale vanishing quadratically with the distance to φ_J. In the following we explore the origin of the anharmonicity responsible for this behavior and offer an explanation for the scaling of $T^\star$ with $|\varphi - \varphi_J|$.

A. Perturbative analysis of high-order nonlinearities

A first natural idea to explain the breakdown of the harmonic approximation is to realize that the harmonic analysis corresponds to a truncation to second order of an expansion of the energy function around a global minimum, which is generally justified if the temperature is low enough. Thus, the emergence of anharmonicity at finite temperature could be due to higher order terms in the expansion becoming relevant.

To explore this hypothesis, we focus on the jammed phase where a genuine harmonic approximation holds, and an expansion of the energy can be performed. To this end, we compute the first low-temperature corrections to the average energy due to higher-order terms, and determine the temperature above which these nonlinearities can no longer be neglected.

We expand the position vector of a particle using a normal mode decomposition defined from a given energy minimum. We write

$$\mathbf{r}_i = \mathbf{r}_i^{(0)} + \sum_a x_a \mathbf{n}_{a,i}, \tag{38}$$

where $\mathbf{r}_i^{(0)}$ is the position of particle in the ground state and $\mathbf{n}_{a,i}$ is the displacement of the i-th particle in the a-th normal mode. Using these normal modes, we can also

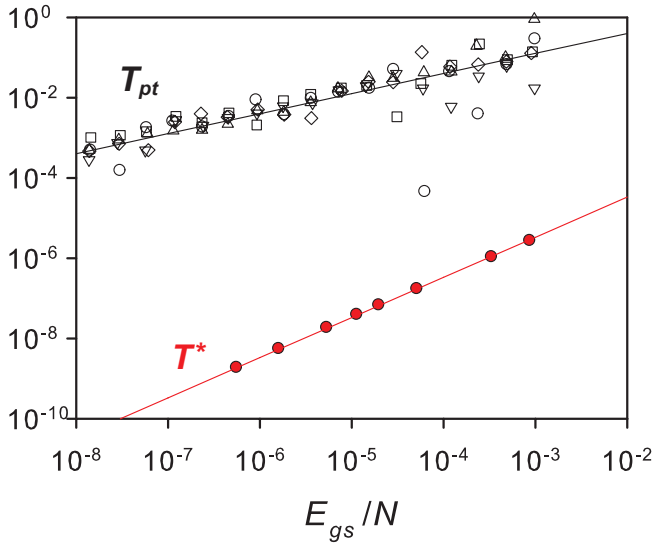

FIG. 10: The crossover temperature scale for the onset of anharmonicity $T^\star$ (bottom data with filled circles) compared to the temperature scale $T_{\rm pt}$ (top data with open symbols different symbols for different packings) quantifying the relevance of the high order terms in the perturvative expansion of the energy. The lines indicate $T^\star \propto E_{\rm gs}$ and $T_{\rm pt} \propto E_{\rm gs}^{1/2}$. Clearly, these two temperature scales differ.

expand the potential energy around the ground state energy into a power series of $\{x_a\}$. Taking the thermal average of this series, we obtain the following temperature expansion form of the potential energy (details of this calculation are reported in the Appendix):

$$\langle E\rangle = E_{\rm gs} + E_1 T + E_2 T^2 + \mathcal{O}(T^3), \tag{39}$$

where $E_{\rm gs}$ is the ground state energy, and

$$E_1 = \frac{1}{2}\sum_{a,b}\frac{\partial^2 V}{\partial x_a \partial x_b}\frac{\delta_{ab}}{\lambda_a} = \frac{3N}{2} \tag{40}$$

$$\begin{aligned} E_2 = & -\frac{1}{8}\sum_{ab}\frac{1}{\lambda_a\lambda_b}\frac{\partial^4 V}{\partial x_a^2 \partial x_b^2} \\ & +\frac{1}{8}\sum_{abc}\frac{1}{\lambda_a\lambda_b\lambda_c}\frac{\partial^3 V}{\partial x_a \partial x_b^2}\frac{\partial^3 V}{\partial x_a \partial x_c^2} \\ & +\frac{1}{12}\sum_{abc}\frac{1}{\lambda_a\lambda_b\lambda_c}\Big(\frac{\partial^3 V}{\partial x_a \partial x_b \partial x_c}\Big)^2. \end{aligned} \tag{41}$$

From these results, we can estimate a characteristic temperature, $T_{\rm pt}$, at which the quadratic term in the temperature expansion becomes equal to the linear one, signalling that a harmonic expansion would break down:

$$T_{\rm pt} = \frac{E_1}{E_2}. \tag{42}$$

We have computed $T_{\rm pt}$ for 10 independent configurations with $N = 256$ particles. Due to the multiple sums in Eq. (41) we are forced to use relatively small system sizes, but we have numerically checked that system size dependence is negligible, or at least much too weak to influence our conclusions. For each configuration, we determine numerically the normal modes at $T = 0$ for various densities above jamming. From the numerical determination of the modes, we estimate E_1 and E_2 in Eqs. (40, 41), and we deduce $T_{\rm pt}$ from Eq. (42). We present our numerical results for $T_{\rm pt}$ in Fig. 10 where it is represented parametrically as a function of the ground state energy, $E_{\rm gs} \propto (\varphi - \varphi_J)^2$. For comparison, we also represent the crossover scale $T^\star$ directly deduced from the study of the density of states $d(\omega)$, as discussed above.

The numerical results indicate that $T_{\rm pt}$ is larger than $T^\star$ at all investigated volume fractions by several orders of magnitude, typically more than a factor 10^4. Also, the density dependence of $T_{\rm pt}$ is quite different from the one of $T^\star$, since the numerical data seem to indicate that $T_{\rm pt} \sim (E_{\rm gs}/N)^{1/2} \sim (\varphi - \varphi_J)$. This means that the harmonic-anharmonic transition observed in the DOS *cannot* be explained through a perturbative analysis around the ground state. These results show that thermally excited packings near jamming are *not* stabilized by quartic terms in the expansion of the energy, and another explanation has therefore to be sought for the existence of $T^\star$.

B. 'Fragility' of contact network and non-analyticity of pair potential

The above calculation is perturbative in nature. It amounts to assuming that when heated, the system will simply explore the energy minimum used to compute the dynamical matrix. Crucially, this reasoning implicitly assumes that the forces are analytic functions, which is not correct for the harmonic pair potential we use which is not analytic in $r = \sigma$ where it is truncated. In fact, the above calculation would hold if $v(r) = (1 - r/\sigma)^2$ for all r-values. Indeed, it was found in Ref. [22] that the threshold for anharmonicity for the non-truncated potential is about 10^4 larger than for the truncated potential. This numerical finding is in fact in quantitative agreement with the results of the previous section, recall the data shown in Fig. 10.

Therefore, we follow Ref. [22] and explore the idea that the change in the DOS observed above $T^\star$ is associated with the breaking and renewal of the 'contact network'. In such case, the anharmonicity would directly result from the non-analyticity in the pair potential. More precisely, it could be that some contacts are lost (or created) when T increases long before the high-order non-linearities become relevant. This physics cannot be described within a perturbative expansion around the ground state and is thus nonperturbative in nature.

In order to get a quantitative estimate of $T^\star$ we must determine the temperature scale for which thermal fluctuations become large enough to disrupt the contact network. We start again with the jammed phase. Our phys-

ical idea is that since overlaps between particles are small close to jamming, they are more rapidly blurred by the effect of thermal vibrations.

Let us now make this idea more precise. At volume fraction $\varphi > \varphi_J$ and $T = 0$, the typical length of the overlap between contacting particles is $\delta_0 = \sigma - |\mathbf{r}_i - \mathbf{r}_j| \approx (\varphi - \varphi_J)$. The latter estimate comes from the scaling of the width of the first peak in the pair correlation function near φ_J. On the other hand, at finite temperature, the overlap between two particles becomes a fluctuating quantity. The typical displacement between two neighboring particles has different scaling depending on the direction, longitudinal (L) or transverse (T), to the bond vector $\mathbf{r}_i - \mathbf{r}_j$ [46]:

$$\delta_L \propto \sqrt{T}, \qquad \delta_T \propto \sqrt{T}\,(\varphi - \varphi_J)^{-1/4}\,. \tag{43}$$

In order to loose a contact one must have either $\delta_L \sim \delta_0$ or $\delta_T \sim \sqrt{\delta_0}$, from purely geometrical reasoning. The first identity is more constraining, and implies that the notion of 'contacts' between particles only makes sense when $\sqrt{T} < (\varphi - \varphi_J)$, which directly explains the scaling of the crossover temperature $T^\star \sim (\varphi - \varphi_J)^2$.

On the hard sphere side below jamming, a similar reasoning holds with the overlap being replaced by the gap between the particles. Note that this argument also implies that the quadratic dependence of $T^\star$ with the distance to φ_J is actually a direct consequence of the exponent in the pairwise interaction potential, which we have considered to be purely harmonic throughout this study.

We can get an even more quantitative grasp of the crossover scale $T^\star$ through an analysis of the radial distribution function $g(r)$. At $T = 0$, $g(r)$ has a sharp peak near $r = \sigma$, and its width is $\delta_0 \simeq 0.4(\varphi - \varphi_J)$, the prefactor being determined numerically. In general, the radial distribution function is a volume average of the radial distribution function around a specific particle,

$$g(r) = \frac{1}{N}\sum_i g_i(r) = \frac{1}{N}\sum_i \left\langle \sum_j \delta(r - |\mathbf{r}_{ij}|) \right\rangle . \tag{44}$$

At $T = 0$, $g_i(r)$ is the sum of delta functions corresponding to the relative distance between particle i and all its neighbors in the studied packing. When $T > 0$, these delta functions broaden under the influence of thermal fluctuations, and thus they acquire a width of the order $\sqrt{T}$ discussed above.

In Fig. 11, we presents numerical results for $g(r)$ and the $g_i(r)$ for a randomly chosen particle i at various temperatures both above and below $T^\star$, which for this example is $T^\star \approx 4 \cdot 10^{-7}$. At $T = 10^{-8}$, $g_i(r)$ shows well-resolved delta functions, while $g(r)$ is close to its $T = 0$ value. With increasing temperature, the peaks in $g_i(r)$ broaden, and cannot be resolved anymore above $T^\star$ when their width becomes comparable to the width of the $T = 0$ width of $g(r)$. At even higher temperature, $T = 10^{-5}$, the overall shape of $g(r)$ is now controlled by the broadening of individual $g_i(r)$, and its shape becomes very different from the structure at $T = 0$, see Ref. [20].

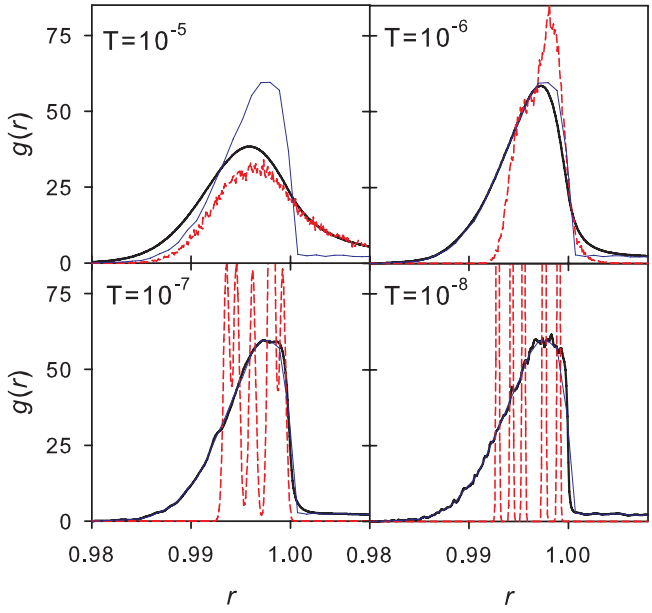

FIG. 11: The radial distribution function $g(r)$ at finite T, (black / thick lines), at $T = 0$ (blue / thin line), and its particle-resolved version $g_i(r)$ (red / dashed lines) for a randomly chosen particle i at $\varphi = 0.66$ and various temperatures. While contacts between i and its neighbors are well-defined at low T, they cannot be resolved when T becomes larger than $T^\star$ which is $\approx 4 \times 10^{-7}$ for this particular density.

Let us push the argument further. Quantitatively, we determine numerically that the thermal broadening of individual peaks in $g_i(r)$ is given by $\simeq 0.9\sqrt{T}$, such that at $T = T^\star$ we obtain a width $\simeq 0.03(\varphi - \varphi_J)$. This should be compared to the width of $g(r)$ at half maximum, $\delta_0 \approx 0.4(\varphi - \varphi_J)$, which is about 10 times larger. This numerical factor is reasonable since each particle possesses on average about 6 neighbors, and so the smallest of these overlaps is about $\delta_0/6 \sim 0.066(\varphi - \varphi_J)$ which is indeed not far from $0.03(\varphi - \varphi_J)$.

Our argument suggests that anharmonicy starts to play a role and modify the DOS when an *extensive* number of contacts become affected by thermal fluctuations. This is at odds with the results in Ref. [22] where a threshold for anharmonicity was defined via the breaking of a *single* contact in a given packing. This qualitative difference in our analysis presumably explains the different conclusion that we reach in this work, namely that a finite regime exists where a harmonic approximation is valid even in the thermodynamic limit, thus contradicting the different claim made in Ref. [22] that the domain of validity of harmonic theory is null.

To summarize, we find that the onset of anharmonicity does not follow from the breakdown of a perturbative expansion to second order, but rather stems from the non-analycity of the pair interaction. Remark that the use of a truncated pair potential is of course a mandatory ingredient for the system to display a jamming transition in the first place. There is thus no room, it would seem,

to make the physics associated to the jamming transition more robust against thermal fluctuations since the very origin of the critical fluctuations—a marginally stable solid with vanishingly small overlaps between particles—also makes it highly sensitive to thermal fluctuations. This conclusion suggests that experimental investigations of the jamming transition using colloidal particles are not straightforward, as we now discuss.

VIII. DISCUSSION: EXPERIMENTS VERSUS THEORY

The theoretical analysis conducted in this article shows that single particle dynamics is able to directly reveal the divergence of time scales and length scales when the jamming transition at ($T = 0$, $\varphi = \varphi_J$) is approached. We have additionnally shown that dynamic criticality survives a finite amount of temperature, and have carefully explained under what conditions the signatures of the jamming singularity remain observable in the dynamics at finite temperature, emphasizing in particular the existence of three distinct critical regimes in the vicinity of the critical point, Fig. 8. We suggested a possible connections between the vibrational heterogeneity unveiled here and the experimental reports in Ref. [26, 27]. Other experiments report a nonmonotonic evolution of dynamic heterogeneity with density [48, 49], but the connection with our work is less clear.

We mentioned in the introduction the important experimental activity in the colloidal community aiming at characterizing the emergence of 'soft modes' near the jamming transition. It is interesting to use our findings to discuss these experimental investigations. Two different types of colloidal systems have been used, which we discuss separately.

A first series of experiments concentrates on colloidal PMMA hard spheres [9, 10, 14]. In that case, temperature simply serves to produce Brownian motion but since particles are 'infinitely' hard, temperature does not blur the jamming transition, and thus these experiments are in principle well-suited to probe Regime II, the critical regime of hard spheres. However, the investigations in Refs. [9, 10] were performed in the range $\varphi = 0.56 - 0.60$. Although some care must be taken with the absolute values of φ in experimental work, these values seem consistent because the amplitude of the experimentally-measured DW factors are in the range $\Delta^2(\infty) \approx (0.005 - 0.03)\sigma^2$, see Fig. 1. However, these volume fractions are very far from φ_J (see Figs. 4 and 5) and all lie outside the critical regime II where a sharp drop in the DW factor would be observed, accompanied by the appearance of low-frequency modes and a growing correlation length. It would therefore be interesting to push these experiments further towards the jamming transition, to see whether experimental signatures of the dynamic criticality discussed in this work can be detected. In Fig. 12, we provide an extended view of the (T, φ) phase diagram including the experimentally explored regime for hard spheres, outside the critical region discussed in our work.

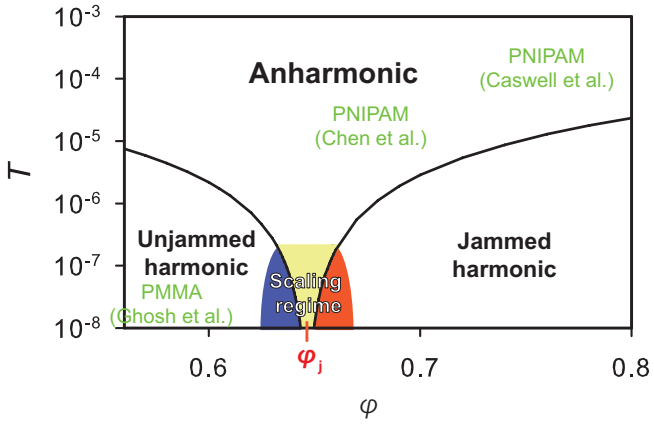

FIG. 12: An enlarged view of the (Temperature, Volume fraction) phase diagram reporting the critical regimes shown in Fig. 8, and the approximate location of the experimental studies aimed at studying anomalous vibrational dynamics in colloidal systems: Gosh *et al.* [9] use PMMA hard spheres, while Chen *et al.* [11] and Caswell *et al.* [15] study PNIPAM microgel particles. Previous studies all lie too far away from the jamming transition to detect the dynamic criticality associated to the transition.

A second series of experiments designed to probe low-frequency modes near jamming uses soft 'PNIPAM' microgel particles [11–13, 15]. In this case both the volume fraction and the temperature, expressed in units of the particle softness, are relevant control parameters. Because microgel particles are easily compressed, the volume fraction can be adjusted to be as close to the jamming density as desired. However, softness is now the main issue. The adimensional temperature estimate is $T/\epsilon \approx 2 \times 10^{-5}$ in Ref. [11]. We can confirm this value by again using the DW factor as a sensitive 'thermometer'. Indeed, the values measured near jamming, $\Delta^2(\infty) \sim 3 \times 10^{-4}\sigma^2$, correspond in our Fig. 1 to a temperature scale of about 10^{-5}. In very recent work with different microgel particles [15], the DW factor is larger, $\Delta^2(\infty) \sim 2 \times 10^{-3}\sigma^2$, and thus the system is effectively at an even higher temperature, of the order 10^{-4}. On the basis of our numerical results, we conclude that the microgel particles studied in Refs. [11, 15] are so soft (or, equivalently so 'hot') that anharmonicity is very strong because temperature is much larger than the crossover scale $T^\star$, see their location in the phase diagram of Fig. 12. As for hard colloids, we suggest that it could be interesting to design different experimental systems with particles that are less soft than microgels, for instance emulsions, in order to probe experimentally the critical dynamics associated to the jamming transition.

In conclusion, because of the smallness of the critical region (that certainly would deserve a theoretical explanation) experiments have not yet probed critical prop-

erties related to the jamming transition. Since they are quite far from the critical region, our results imply that there cannot be any direct connection between the DOS measured in those experiments and the theoretical results established at $T = 0$. On the basis of our results, one should find an alternative explanation, not based on 'thermal vestiges' of the jamming transition, for the experimental results. Indeed, there is no need to invoke any critical behavior to account for the smooth evolution with density of the low-frequency $\omega^\star$ reported in Ref. [11]. It is fully consistent with the data obtained in Fig. 2 for large temperatures which basically track the microscopic time scale τ_0 that changes smoothly across φ_J as a direct result of the compression. Another experimental signature of the jamming singularity is the nonmonotonic evolution of the pair correlation upon compression [15, 47]. This can also be explained in a way unrelated to the critical properties of the jamming transition since, as demonstrated in Ref. [19], this anomaly persists arbitrarily far from the transition, even in the equilibrium fluid.

In conclusion, our study reveals that single particle motion in thermal systems near jamming becomes singular, and reveals a number of scaling laws and divergences for both time scales and length scales. This dynamic criticality thus provides direct evidence of the critical nature of the jamming transition occurring at $T = 0$, and might suggest new routes to attack the problem from a theoretical viewpoint, for instance using the replica approach in the framework of statistical mechanics. In addition, we have suggested that it would be very interesting to design new experiments using colloidal systems to probe more closely the diverging time scales and length scales associated to vibrational dynamics of dense packings.

Acknowledgments

We thank O. Dauchot, C. Goodrich, and F. Zamponi for useful discussions. Our work is supported by Région Languedoc-Roussillon (AI, LB), and from ERC grant NPRG-GLASS (GB).

Appendix A: Derivation of Eqs. (39 - 41)

Using the normal modes decomposition of the position vector of a particle Eq. (38), the potential energy of the system can be expanded as

$$E = E_{\rm gs} + \frac{1}{2}\sum_{ab} V_{ab}x_a x_b + \frac{1}{3!}\sum_{abc} V_{abc}x_a x_b x_c + \frac{1}{4!}\sum_{abcd} V_{abcd}x_a x_b x_c x_d + \mathcal{O}(x^5), \quad \text{(A1)}$$

where we introduced a simplified notation for the derivatives, e.g. $V_{ab} = \frac{\partial^2 v}{\partial x_a \partial x_b}$. Note that the first order term vanishes since we focus on a potential energy minimum. We regard this development of the potential energy as the sum of the harmonic term E_0 (up to second order) and anharmonic terms ΔE. When ΔE is treated as perturbation, we can obtain the following expansion of the distribution function,

$$f = f_0\Big(1 - \beta(\Delta E - \langle\Delta E\rangle_0) + 1/2\beta^2(\Delta E^2 - \langle\Delta E^2\rangle_0 - 2\Delta E\langle\Delta E\rangle_0 + 2\langle\Delta E\rangle_0^2) + \mathcal{O}(\beta^3\Delta E^3)\Big), \quad \text{(A2)}$$

where f is the canonical distribution function corresponding to E and f_0 to E_0; $\langle\cdots\rangle_0$ indicates a thermal average over the distribution f_0. Taking the thermal average of Eq. (A1) using the distribution function in Eq. (A2), we obtain the perturbation expansion of the potential energy.

To organize this series as the low-temperature expansion, we have estimated the temperature dependence of each term using the fact that $\langle x^n\rangle_0 \propto T^{n/2}$ when n is even. As a result, we get the following equation:

$$\langle E\rangle = E_{gs} + \frac{1}{2}\sum_{ab} V_{ab}\langle x_a x_b\rangle_0 + \frac{1}{4!}\sum_{abcd} V_{abcd}\langle x_a x_b x_c x_d\rangle_0 - \frac{1}{T}\sum_{abcdef}\Big(\frac{1}{3!3!}V_{abc}V_{def}\langle x_a x_b x_c x_d x_e x_f\rangle_0 + \frac{1}{2!4!}V_{ab}V_{cdef}\langle x_a x_b x_c x_d x_e x_f\rangle_0 - \frac{1}{2!4!}V_{ab}V_{cdef}\langle x_a x_b\rangle_0\langle x_c x_d x_d x_f\rangle_0)\Big) + \frac{1}{2T^2}\sum_{abcdefgh}\frac{1}{2!3!3!}V_{ab}V_{cde}V_{fgh}\Big(\langle x_a x_b x_c x_d x_e x_f x_g x_h\rangle_0 - \langle x_a x_b\rangle_0\langle x_c x_d x_e x_f x_g x_h\rangle_0\Big) + \mathcal{O}(T^3), \quad \text{(A3)}$$

where the first term is constant, the second term is proportional to T, the next 6 terms are $\mathcal{O}(T^2)$, and the rest is $\mathcal{O}(T^3)$. Although four-, six- and eight-point functions appear in this expression, they can be evaluated using the Gaussian approximation and Wick's theorem. For example, the expectation value of the two-point function is simply

$$\langle x_a x_b\rangle_0 = \frac{\delta_{ab}T}{\lambda_a}, \quad \text{(A4)}$$

where λ_a is the eigenvalue for the a-th normal modes. Note also that the second order derivatives are the diagonal matrix $V_{ab} = \lambda_a \delta_{ab}$. Using these relations with Wick's theorem, we obtain the final expressions in Eqs. (39-41).

[1] A. J. Liu, M. Wyart, W. van Saarloos and S. R. Nagel in *Dynamical heterogeneities in glasses, colloids and granular materials*, Eds.: L. Berthier, G. Biroli, J.-P. Bouchaud, L. Cipelletti, and W. van Saarloos, (Oxford University Press, Oxford, 2011).

[2] M. Wyart, L. Silbert, S. R. Nagel, and T. A. Witten, Phys. Rev. E **72**, 051306 (2005).

[3] L. E. Silbert, A. J. Liu, and S. R. Nagel, Phys. Rev. Lett. **95**, 098301 (2005).

[4] L. Wang and N. Xu, arXiv:1112.2429.

[5] N. Xu, V. Vitelli, A. J. Liu and S. R. Nagel, Europhys. Lett. **90**, 56001 (2010).

[6] V. Vitelli, N. Xu, M. Wyart, A. J. Liu, and S. R. Nagel, Phys. Rev. E **81**, 021301 (2010).

[7] G. Düring, E. Lerner, and M. Wyart, arXiv:1204.3542.

[8] C. Brito and M. Wyart, J. Chem. Phys. **131**, 024504 (2009).

[9] A. Ghosh, V. K. Chikkadi, P. Schall, J. Kurchan, and D. Bonn, Phys. Rev. Lett. **104**, 248305 (2010).

[10] A. Ghosh, R. Mari, V. Chikkadi, P. Schall, J. Kurchan, and D. Bonn, Soft matter **6**, 3082 (2010).

[11] K. Chen, W. G. Ellenbroek, Z. Zhang, D. T. N. Chen, P. J. Yunker, C. Brito, O. Dauchot, S. Henkes, W. van Saarloos, A. J. Liu, and A. G. Yodh, Phys. Rev. Lett. **105**, 025501 (2010).

[12] D. Kaya, N. Green, C. E. Maloney and M. F. Islam. Science **329**, 656 (2010).

[13] D. Kaya, N. Green, C. E. Maloney and M. F. Islam. Phys. Rev. E **83**, 051404 (2011).

[14] P. Tan, N. Xu, A. B. Schofield, and L. Xu, Phys. Rev. Lett. **108**, 095501 (2012).

[15] T. A. Caswell, Z. Zhang, M. L. Gardel, S. R. Nagel, arXiv:1206.6802 (2012).

[16] C. Brito, O. Dauchot, G. Biroli, and J.-P. Bouchaud, Soft Matter **6**, 3013 (2010).

[17] P. M. Chaikin and T. C. Lubensky, *Principles of Condensed Matter Physics*, (Cambridge University Press, Cambridge, 1995).

[18] L. Berthier and T. A. Witten, EPL **86**, 10001 (2009); Phys. Rev. E **80**, 021502 (2009).

[19] H. Jacquin and L. Berthier, Soft Matter **6**, 2970 (2010).

[20] L. Berthier, H. Jacquin, and F. Zamponi, Phys. Rev. E **84**, 051103 (2011); J. Stat. Mech. P01004 (2011).

[21] M. Otsuki and H. Hayakawa, arXiv:1111.1313

[22] C. F. Schreck, T. Bertrand, C. S. O'Hern, and M. D. Shattuck, Phys. Rev. Lett. **107**, 078301 (2011).

[23] S. Henkes, C. Brito and O. Dauchot, Soft Matter **8**, 6092 (2012).

[24] G. Parisi and F. Zamponi, Rev. Mod. Phys. **82**, 789 (2010).

[25] H. Jacquin, L. Berthier, and F. Zamponi, Phys. Rev. Lett. **106**, 135702 (2011).

[26] F. Lechenault, O. Dauchot, G. Biroli, and J.-P. Bouchaud, Europhys. Lett. **83**, 46002 (2008).

[27] C. Coulais, R. P. Behringer, and O. Dauchot, arXiv:1202.5687.

[28] W. G. Ellenbroek, E. Somfai, M. van Hecke, W. van Saarloos, Phys. Rev. Lett. **97**, 258001 (2006).

[29] D. J. Durian, Phys. Rev. Lett. **75**, 4780 (1995).

[30] C. S. O'Hern, S. A. Langer, A. J. Liu, and S. R. Nagel, Phys. Rev. Lett. **88**, 075507 (2002).

[31] P. Chaudhuri, L. Berthier, and S. Sastry, Phys. Rev. Lett. **104**, 165701 (2010).

[32] P. Olsson and S. Teitel, Phys. Rev. Lett. **99**, 178001 (2007).

[33] C. Heussinger, L. Berthier, and J.-L. Barrat, EPL **90**, 20005 (2010).

[34] A. Ikeda, L. Berthier, and P. Sollich, Phys. Rev. Lett. **109**, 018301 (2012).

[35] L. Berthier and G. Biroli, Rev. Mod. Phys. **83**, 587 (2011).

[36] G. S. Grest, S. R. Nagel, A. Rahman, and T. A. Witten, J. Chem. Phys. **74**, 3532 (1981).

[37] J. P. Hansen and I. R. McDonald, *Theory of Simple Liquids*, (Elsevier, Amsterdam, 1986).

[38] L. Berthier, G. Biroli, J.-P. Bouchaud, and R. L. Jack, in *Dynamical heterogeneities in glasses, colloids, and granular media*, Eds.: L. Berthier, G. Biroli, J.-P. Bouchaud, L. Cipelletti, and W. van Saarloos, (Oxford University Press, Oxford, 2011).

[39] C. Toninelli, M. Wyart, L. Berthier, G. Biroli, and J.-P. Bouchaud, Phys. Rev. E **71**, 041505 (2005).

[40] L. Berthier, G. Biroli, J.-P. Bouchaud, W. Kob, K. Miyazaki, and D. Reichman, J. Chem. Phys. **126**, 184503 (2007); J. Chem. Phys. **126**, 184504 (2007).

[41] P. C. Hohenberg and B. I. Halperin, Rev. Mod. Phys. **49**, 435 (1977).

[42] T. Hatano, Phys. Rev. E **79**, 050301(R) (2009).

[43] J. A. Drocco, M. B. Hastings, C. J. Olson Reichhardt, and C. Reichhardt, Phys.Rev. Lett. **95**, 088001 (2005).

[44] J. Kurchan, G. Parisi, and F. Zamponi, arXiv:1208.0421

[45] L. R. Gómez, A. M. Turner, M. van Hecke, and V. Vitelli, Phys. Rev. Lett. **108**, 058001 (2012).

[46] W.G. Ellenbroek, E. Somfai, M. van Hecke, W. van Saarloos, Phys. Rev. Lett. **97** 258001 (2006).

[47] Z. Zhang, N. Xu, D. T. N. Chen, P. Yunker, A. M. Alsayed, K. B. Aptowicz, P. Habdas, A. J. Liu, S. R. Nagel, and A. G. Yodh, Nature **459**, 230 (2009).

[48] P. Ballesta, A. Duri, and L. Cipelletti, Nature Phys. **4**, 550 (2008).

[49] D. A. Sessoms, I. Bischofberger, L. Cipelletti, and V. Trappe, Phil. Trans. R. Soc. A **367**, 5013 (2009).

[50] Note that these arguments hold even with less restrictive assumptions; one simply needs that $f(x)$ does not increase faster than x when $x \to \infty$, but the specific form of $f_{\pm}(x)$ is irrelevant.

[51] It would not make sense to renormalize the wavevector in $S_4(q)$, and thus χ_4, in terms of ℓ_0 since the dynamic correlation length corresponds to the number of spatially correlated particles and is not related to the scale over which single particles move.